

Efficient Identifying the Orientation of Single NV Centers in Diamond and Using them to Detect Near Field Microwave

Xuerui Song,^{1, a)} Fupan Feng,^{1, b)} Chunxiao Cai,¹ Guanzhong Wang,² Wei Zhu,² Wenting Diao,¹ and Chongdi Duan¹

¹⁾ China Academy of Space Technology (Xi'an), Xi'an, Shaanxi, 710100, P. R. China

²⁾ Hefei National Laboratory for Physical Science at Microscale, and Department of Physics, University of Science and Technology of China, Hefei, Anhui, 230026, P. R. China

Arrays of NV centers in the diamond have the potential in the fields of chip-scale quantum information processing and nanoscale quantum sensing. However, determining their orientations one by one is resource intensive and time consuming. Here, in this paper, by combining scanning confocal fluorescence images and optical detected magnetic resonance, we realized a method of identifying single NV centers with the same orientation, which is practicable and high efficiency. In the proof of principle experiment, five single NV centers with the same orientation in a NV center array were identified. After that, using the five single NV centers, microwave near field generated by a $20\mu\text{m}$ -diameter Cu antenna was also measured by reading the fluorescence intensity change and Rabi frequency at different microwave source power. The gradient of near field microwave at sub-microscale can be resolved by using array of NV centers in our work. This work promotes the quantum sensing using arrays of NV centers.

Nitrogen-vacancy(NV) centers are paramagnetic defects within the diamond lattice, which consist of a substitutional N impurity adjacent to a vacant lattice site. Owing to their outstanding optical and spin properties at room temperature, NV centers have attracted more and more attentions in the fields of nanoscale quantum sensing and quantum information processing.¹⁻⁶ Especially in the fields of quantum sensing, due to the fact that the NV center can be stably located close to the diamond surface at nanoscale or nanodiamonds,⁷⁻¹⁰ the spatial resolution of the sensors based on NV centers have down to nanoscale.^{3,11-13} This nanoscale property is quite important in the fields of condensed matter physics and biology research.¹⁴⁻¹⁷ Recently, some groups reported that the near field microwave(MW) sensing using NV centers in diamond have down to micro even nanoscale resolutions.¹⁸⁻²⁴

Precise detecting of the spatial distribution of the MW near field is crucial for developing new types of MW devices, chip failure checking, electromagnetic compatibility analyzing and even solid state physics studying.²⁵ Generally speaking, the spatial resolution of the traditional dipole probe is limited to about $100\mu\text{m}$. Even worse, during the MW measuring process, the dipole probe will reconstruct the electromagnetic field, which can disturb the near field detection.²⁶ In recent years, new sensors based on alkali vapor cell, superconductor and spin-torque diode have been developed to detect the near field MW with high sensitivity.²⁷⁻²⁹ However, none of them obtained nanoscale spatial resolution. The development of near field MW sensors based on NV center will bring an ultimate solution to this problem.

As shown in the right section of Fig. 1, the ground state of electron spin of the NV center is a spin triplet 3A_2

with a zero field splitting of $D = 2.87\text{GHz}$. The oscillation between $|0\rangle$ and $|\pm 1\rangle$ ground states can be driven by a resonant MW magnetic field as $\hbar\omega = D \pm \gamma B_Z$, where B_Z is a static magnetic field along the axis of NV center, $\gamma = 2.8025\text{MHz/Gauss}$ is the gyromagnetic ratio of the electron spin. The MW magnetic field is written as $\mathbf{B}_{MW}(t) = \mathbf{B}_{MW}\cos(\omega t)$, where $f = \frac{\omega}{2\pi}$ is the MW frequency. By carrying out the optical detected magnetic resonant (ODMR), the resonant frequency of the MW field can be obtained. By adding static magnetic field \mathbf{B} , $|\pm 1\rangle$ can be further splitted, which varies the resonant MW field frequency from kHz to sub-THz.³⁰ Additionally, the Rabi frequency of the spin state oscillation Ω is proportional to the component of the MW field in a plane perpendicular to the NV axis as $\Omega = \gamma B_{MW\perp}$. At last, by using NV centres at the four different axes, the total amplitude B_{MW} and the orientation of the vector can be obtained by measuring different $B_{MW\perp}$. By doing this, noninvasive detecting of near field MW magnetic field at nanoscale resolution obtained.^{18,19}

Traditionally, to measure field at nanoscale resolution, scanning should be carried out by combining the NV sensors with AFM tip, which is highly requirement in practice.^{9,19,31} Alternatively, by measuring field using NV centers at different sites, NV center arrays in the diamond have the potential in the fields nanoscale quantum sensing.³²⁻³⁴ However, determining their orientations one by one is resource intensive and time consuming. In this work, using shallow NV center arrays in diamond, a method by combining scanning confocal fluorescence image and optical detected magnetic resonance was developed to efficiently identify the NV centers with same orientation. The relative MW amplitude distribution is obtained by measuring the fluorescence intensity and the Rabi oscillation of the single NV center at different sites of the arrays. The spatial resolution of near field MW sensors based on array of NV centers in this work is hundreds of nanometers which consists with the

^{a)} Electronic mail: songxr@cast504.com

^{b)} Electronic mail: fengfp@cast504.com

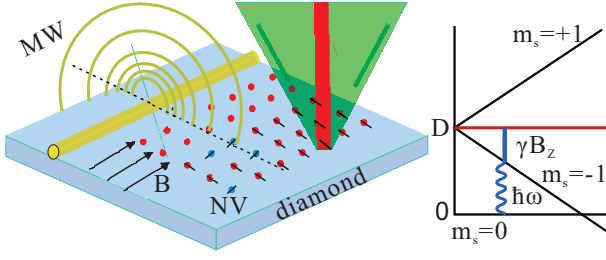


Figure 1. Experiments and principle illustrating of the work. Left, shallow array of NV centers with different orientations were located close to the diamond surface within nanometers. The near field MW was generated by a $20\ \mu\text{m}$ -diameter Cu antenna which lays tens of micrometers above the diamond surface. The NV center was excited by $532\ \text{nm}$ green laser. The red fluorescence was collected by an objective and then detected by an APD. Right, energy level of the ground state of the electron spin of NV center.

optical microscope.

The sample used in this work was a $2 \times 2 \times 0.5\ \text{mm}^3$ high-quality electronic grade diamond with natural isotopic concentration of ^{13}C (1.1%) from Element Six. The NV center array was prepared by implanting $8\ \text{keV}$ $^{14}\text{N}_2^+$ molecules with a fluence of $8 \times 10^{10}\ \text{N}_2^+/\text{cm}^2$. The implantation angle is 7° through $60\ \text{nm}$ diameter apertures which were patterned using electron beam lithography in a 300-nm -thick polymethyl methacrylate (PMMA) layer deposited on the diamond surface.^{33,35,36} After implantation, the sample was annealed $2\ \text{h}$ at 1050°C in a vacuum at $2 \times 10^{-5}\ \text{Pa}$ to induce vacancy diffusion to form NV centers. According to SRIM simulation of the stopping of nitrogen ions in diamond chip, the most probable stopping position of the implanted nitrogen ions was $6.5\ \text{nm}$ below the diamond surface.³⁷ After preparation of the NV center arrays, the diamond sample was placed in the setup shown in Fig.1. The scanning confocal fluorescence image of the NV center array with a $10 \times 10\ \mu\text{m}^2$ region was shown in Fig. 2(a). The fluence of the $^{14}\text{N}_2^+$ molecules and the size of the apertures used during the implantation ensure that most of the bright spots in the arrays was single NV center, which is consistent with the ODMR experiments. It should be noted that due to the low energy of the implanting ions, creation of the NV centers were unsuccessful in some sites.

Then, by combining scanning confocal fluorescence image and optical detected magnetic resonance, we realized a method which can fast identify single NV centers with the same orientation, so called scanning optical detected magnetic resonance (SODMR) method. By sweeping the MW frequency using the $20\ \mu\text{m}$ -diameter Cu antenna under continuous $532\ \text{nm}$ green laser excitation, the ODMR of a single NV center that randomly selected (pointed by a black arrow in Fig. 2(a)) under zero magnetic field was measured. The dip of the ODMR spectrum (Fig. 2(b)) located at $2.87\ \text{GHz}$ corresponds to the transition between $|0\rangle$ and $|\pm 1\rangle$ states. After that, a static magnetic field \mathbf{B} generated by an electromagnet was applied

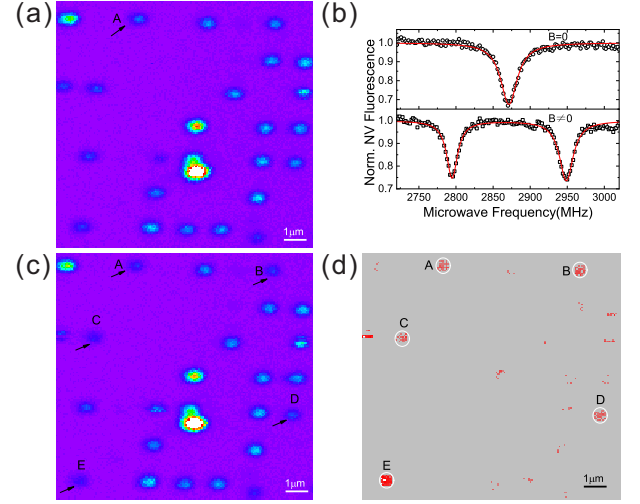


Figure 2. Efficient identifying the orientation of NV centres in diamond. (a) Scanning confocal fluorescence image of NV center array with a $10 \times 10\ \mu\text{m}^2$ region. (b) ODMR spectrum of the NV center as pointed in Fig. 2(a). Upper spectrum, $B = 0$. Lower spectrum, $B \neq 0$. (c) Under continuous MW excitation with resonance frequency at $2.794\ \text{GHz}$ ($2.949\ \text{GHz}$), the scanning confocal fluorescence image of the region of Fig. 2(a) was recorded again. (d) Imaging of the five single NV centers with the same orientation.

to the NV center to further split the $|\pm 1\rangle$ states. At this condition, as shown in lower spectrum of Fig. 2(b), the two dips located at $2.794\ \text{GHz}$ and $2.949\ \text{GHz}$ correspond to the transitions of $|0\rangle \leftrightarrow | -1\rangle$ and $|0\rangle \leftrightarrow | +1\rangle$ respectively. As the resonance frequency of the A-point is known, the NV centers with the same orientation can be identified immediately by our SODMR method introduced here. By applying continuous MW excitation at $2.794\ \text{GHz}$ ($2.949\ \text{GHz}$), the scanning confocal fluorescence image of the same region of Fig. 2(a) was recorded again. The dramatically decreased fluorescence intensity of the A-point in Fig. 2(c) confirmed that magnetic resonance occurred during scanning counting of the fluorescence of A. As same as A, the fluorescence intensity of the other four single NV centers marked as B, C, D and E, which have the same orientation as A, also decreased. As a comparison, the fluorescence intensity of the other NV centers, which have different orientation with A, showed little change. To further improve the efficiency of identifying of the NV centers with the same orientation, the contrast diagram of the fluorescence intensity was normalized as $\frac{I_{\text{res}} - I_{\text{no-MW}}}{I_{\text{no-MW}}}$, where I_{res} (Fig. 2(c)) was the fluorescence of NV centers under microwave radiation and $I_{\text{no-MW}}$ (Fig. 2(a)) was that of without MW. As shown in Fig. 2(d), five of the single NV centers with the same orientation obviously displayed. The method of identifying of the single NV centers with the same orientation introduced here is more efficiency for arrays with a mass of NV centers.^{36,38}

As has been reported, the MW power influences the

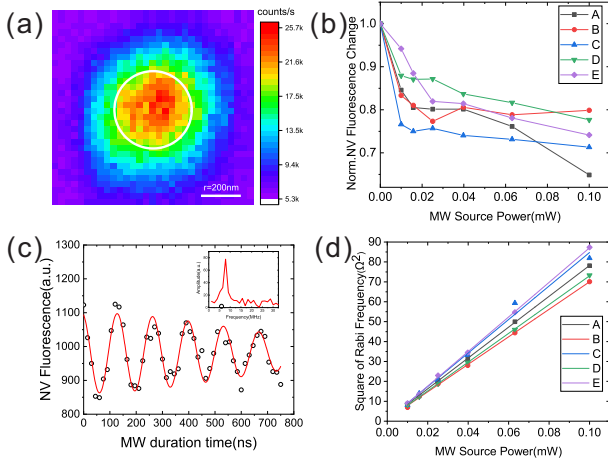


Figure 3. Using the five NV centers identified, MW near field generated by a $20\mu\text{m}$ -diameter Cu antenna was measured. (a) Scanning confocal fluorescence image of one of the single NV center at MW power of 0.04 mW . (b) NV fluorescence change VS MW source power. (c) Example of Rabi oscillation of single NV center. Insert, FFT of the Rabi oscillation. (d) Square of Rabi frequency (Ω^2) versus MW source power.

contrast of the ODMR spectrum.^{39,40} Therefore, on the condition of resonance, the power of MW near field can be indirectly read out by measuring the fluorescence intensity change of the NV centers.^{19,41} Utilizing the five NV centers with the same orientation identified above, the relative component of the MW field amplitude in a plane perpendicular to the NV axis $B_{MW\perp}$ was studied by measuring the fluorescence intensity and Rabi oscillation frequency Ω . Fig. 3(a) shows the scanning confocal fluorescence image of single NV center at MW power of 0.04 mW . The corresponding fluorescence intensity was obtained by sum the total counts within a circle around the center of fluorescence spot with a radius of 200 nm . Fig. 3(c) shows an example of the Rabi oscillation, and the Rabi frequency was obtained by carrying out the FFT of the data (insert in Fig. 3(c)). The measured projected fluorescence intensity and square of Rabi frequency (Ω^2) versus MW source power were shown in Fig. 3(b) and Fig. 3(d) respectively. From Fig. 3(b) we can see that, with the increasing of the MW source power from 0 to 0.02 mW , the NV fluorescence intensity sharply decreased. From 0.02 to 0.1 mW , the fluorescence intensity decreased steadily, indicating that a saturation effect exists under strong MW source power.⁴⁰ This result demonstrated that the method of measuring the relative MW intensity by reading the NV fluorescence intensity change is more faithful under weaker MW power excitation. Additionally, under strong MW excitation (e.g. 0.1 mW), the NV fluorescence intensity change of A, C, E is more obvious than B and D, which is consistent with the fact that the later two NV centers are more far-away from the Cu MW antenna, as the configuration shown in Fig. 1 and Fig. 2(c). Fig. 3(d) shows the proportional relationship of the square of Rabi frequency

(Ω^2) versus MW source power as $\Omega^2 \propto P$. The result data were fitted by linearity curves. The gradient of the MW was precisely reflected by the slopes of the linearity curves as $E > C > A > D > B$, which is consistent with the configuration of the five NV centers shown in Fig. 2(c), except for the spot of B. The unusual of spot B was also shown in the Fig. 3(b) under strong MW power (e.g. 0.1 mW), which indicated the distribution of MW near field is not simply linearity with the distance of the antenna.¹⁹ The result indicated that the gradient of near field MW at sub-microscale can be resolved by using array of NV centers in our work. In this paper, only the relative MW amplitude component perpendicular to the quantum axis of the five NV centers with the same orientation was obtained. The MW amplitude vector can be reconstructed by further measuring the Rabi frequency or fluorescence intensity change by using the NV centers in other three axis.¹⁸ In this work, near field MW was detected by reading the fluorescence intensity change and Rabi frequency. Compared with the method by reading the fluorescence intensity change, the method by detecting the Rabi frequency is more convincing to reflect the distribution of the near field MW at high power.

In conclusion, by combining scanning confocal fluorescence images and optical detected magnetic resonance, we realized a method which can fast identify single NV centers with the same orientation. By using an array of single NV center in diamond, five single NV centers with the same axis were identified in a $10 \times 10\mu\text{m}^2$ region which demonstrated that the method is practicable and high efficiency. After that, the relative component of the MW field amplitude in a plane perpendicular to the NV axis was studied by measuring the fluorescence intensity and Rabi oscillation frequency. The gradient of near field MW at sub-microscale can be resolved by using array of NV centers in our work. The method of identifying the orientation of single NV centres in diamond introduced here can also be used to classify spins with different orientations in other solid crystals such as SiC.⁴² By designing the unique configuration, the near field MW sensor using the NV center array introduced here have the potential in the field of chip failure checking.

ACKNOWLEDGMENTS

This work was supported by the Natural Science Foundation of China (Grant No. 11505135 and No. 61501368) and the National Key Laboratory Foundation (Grant No. 6142411185307).

REFERENCES

- C. L. Degen, F. Reinhard, and P. Cappellaro, Reviews of Modern Physics **89**, 035002 (2017).
- J. R. Maze, P. L. Stanwix, J. S. Hodges, S. Hong, J. M. Taylor, P. Cappellaro, L. Jiang, M. V. G. Dutt, E. Togan, A. S. Zibrov,

- A. Yacoby, R. L. Walsworth, and M. D. Lukin, *Nature* **455**, 644 (2008).
- ³A. Ariyaratne, D. Bluvstein, B. A. Myers, and A. C. B. Jayich, *Nature Communications* **9**, 2406 (2018).
- ⁴P. C. Maurer, G. Kucsko, C. Latta, L. Jiang, N. Y. Yao, S. D. Bennett, F. Pastawski, D. Hunger, N. Chisholm, M. Markham, D. J. Twitchen, J. I. Cirac, and M. D. Lukin, *Science* **336**, 1283 (2012).
- ⁵C. E. Bradley, J. Randall, M. H. Abobeih, R. C. Berrevoets, M. J. Degen, M. A. Bakker, M. Markham, D. J. Twitchen, and T. H. Taminiau, *Physical Review X* **9**, 031045 (2019).
- ⁶S. Zaiser, T. Rendler, I. Jakobi, T. Wolf, S.-Y. Lee, S. Wagner, V. Bergholm, T. Schulte-Herbrüggen, P. Neumann, and J. Wrachtrup, *Nature Communications* **7**, 1 (2016).
- ⁷V. Y. Osipov, F. Treussart, S. A. Zargaleh, K. Takai, F. M. Shakhov, B. T. Hogan, and A. Baldycheva, *Nanoscale Research Letters* **14**, 279 (2019).
- ⁸X. Song, G. Wang, X. Liu, F. Feng, J. Wang, L. Lou, and W. Zhu, *Applied Physics Letters* **102**, 133109 (2013).
- ⁹P. Maletinsky, S. Hong, M. S. Grinolds, B. Hausmann, M. D. Lukin, R. L. Walsworth, M. Loncar, and A. Yacoby, *Nature Nanotechnology* **7**, 320 (2012).
- ¹⁰B. K. Ofori-Okai, S. Pezzagna, K. Chang, M. Loretz, R. Schirhagl, Y. Tao, B. A. Moores, K. Groot-Berning, J. Meijer, and C. L. Degen, *Physical Review B* **86**, 081406 (2012).
- ¹¹L. T. Hall, J. H. Cole, C. D. Hill, and L. C. L. Hollenberg, *Physical Review Letters* **103**, 220802 (2009).
- ¹²G. Kucsko, P. C. Maurer, N. Y. Yao, M. Kubo, H. J. Noh, P. K. Lo, H. Park, and M. D. Lukin, *Nature* **500**, 54 (2013).
- ¹³S. Schmitt, T. Gefen, F. M. Stürner, T. Uden, G. Wolff, C. Müller, J. Scheuer, B. Naydenov, M. Markham, and S. Pezzagna, *Science* **356**, 832 (2017).
- ¹⁴F. Casola, T. v. d. Sar, and A. Yacoby, *Nature Reviews Materials* **3**, 1 (2018).
- ¹⁵Y. Wu, F. Jelezko, M. B. Plenio, and T. Weil, *Angewandte Chemie International Edition* **55**, 6586 (2016).
- ¹⁶F. Shi, F. Kong, P. Zhao, X. Zhang, M. Chen, S. Chen, Q. Zhang, M. Wang, X. Ye, Z. Wang, Z. Qin, X. Rong, J. Su, P. Wang, P. Z. Qin, and J. Du, *Nature Methods* **15**, 697 (2018).
- ¹⁷S. E. Lillie, N. Dontschuk, D. A. Broadway, D. L. Creedon, L. C. L. Hollenberg, and J.-P. Tetienne, arXiv:1905.12873 [cond-mat, physics:physics] (2019), arXiv: 1905.12873.
- ¹⁸P. Wang, Z. Yuan, P. Huang, X. Rong, M. Wang, X. Xu, C. Duan, C. Ju, F. Shi, and J. Du, *Nature Communications* **6**, 1 (2015).
- ¹⁹P. Appel, M. Ganzhorn, E. Neu, and P. Maletinsky, *New Journal of Physics* **17**, 112001 (2015).
- ²⁰L. Shao, R. Liu, M. Zhang, A. V. Shneidman, X. Audier, M. Markham, H. Dhillon, D. J. Twitchen, Y.-F. Xiao, and M. Loncar, *Advanced Optical Materials* **4**, 1075 (2016).
- ²¹M. M. Dong, Z. Z. Hu, Y. Liu, B. Yang, Y. J. Wang, and G. X. Du, *Applied Physics Letters* **113**, 131105 (2018).
- ²²A. Horsley, P. Appel, J. Wolters, J. Achard, A. Tallaire, P. Maletinsky, and P. Treutlein, *Physical Review Applied* **10**, 044039 (2018).
- ²³G. Mariani, S. Nomoto, S. Kashiwaya, and S. Nomura, arXiv:1812.02864 [cond-mat, physics:quant-ph] (2018), arXiv: 1812.02864.
- ²⁴M. Chipaux, L. Toraille, C. Larat, L. Morvan, S. Pezzagna, J. Meijer, and T. Debuisschert, *Applied Physics Letters* **107**, 233502 (2015).
- ²⁵A. Wallraff, D. I. Schuster, A. Blais, L. Frunzio, R.-S. Huang, J. Majer, S. Kumar, S. M. Girvin, and R. J. Schoelkopf, *Nature* **431**, 162 (2004).
- ²⁶C. L. Holloway, J. A. Gordon, S. Jefferts, A. Schwarzkopf, D. A. Anderson, S. A. Miller, N. Thaicharoen, and G. Raithel, *IEEE Transactions on Antennas and Propagation* **62**, 6169 (2014).
- ²⁷B. Fang, M. Carpentieri, X. Hao, H. Jiang, J. A. Katine, I. N. Krivorotov, B. Ocker, J. Langer, K. L. Wang, B. Zhang, B. Azzerboni, P. K. Amiri, G. Finocchio, and Z. Zeng, *Nature Communications* **7**, 1 (2016).
- ²⁸F. Couëdo, E. Recoba Pawlowski, J. Kermorvant, J. Trastoy, J. Crété, Y. Lemaître, B. Marcilhac, C. Ulysse, C. Feuillet-Palma, N. Bergeal, and J. Lesueur, *Applied Physics Letters* **114**, 192602 (2019).
- ²⁹H. Fan, S. Kumar, J. Sheng, J. P. Shaffer, C. L. Holloway, and J. A. Gordon, *Physical Review Applied* **4**, 044015 (2015).
- ³⁰N. Aslam, M. Pfender, R. Stöhr, P. Neumann, M. Scheffler, H. Sumiya, H. Abe, S. Onoda, T. Ohshima, J. Isoya, and J. Wrachtrup, *Review of Scientific Instruments* **86**, 064704 (2015).
- ³¹C. L. Degen, *Applied Physics Letters* **92**, 243111 (2008).
- ³²S. A. Momenzadeh, R. J. Stöhr, F. F. de Oliveira, A. Brunner, A. Denisenko, S. Yang, F. Reinhard, and J. Wrachtrup, *Nano Letters* **15**, 165 (2015).
- ³³J. Wang, F. Feng, J. Zhang, J. Chen, Z. Zheng, L. Guo, W. Zhang, X. Song, G. Guo, L. Fan, C. Zou, L. Lou, W. Zhu, and G. Wang, *Physical Review B* **91**, 155404 (2015).
- ³⁴M. Fukami, C. Yale, P. Andrich, X. Liu, F. Heremans, P. Nealey, and D. Awschalom, *Physical Review Applied* **12**, 014042 (2019).
- ³⁵F. Feng, J. Wang, W. Zhang, J. Zhang, L. Lou, W. Zhu, and G. Wang, *Applied Physics A* **122**, 944 (2016).
- ³⁶D. M. Toyli, C. D. Weis, G. D. Fuchs, T. Schenkel, and D. D. Awschalom, *Nano Letters* **10**, 3168 (2010).
- ³⁷J. F. Ziegler, M. D. Ziegler, and J. P. Biersack, *Nuclear Instruments and Methods in Physics Research Section B: Beam Interactions with Materials and Atoms 19th International Conference on Ion Beam Analysis*, **268**, 1818 (2010).
- ³⁸B. J. M. Hausmann, T. M. Babinec, J. T. Choy, J. S. Hodges, S. Hong, I. Bulu, A. Yacoby, M. D. Lukin, and M. Loncar, *New Journal of Physics* **13**, 045004 (2011).
- ³⁹K. Jensen, V. M. Acosta, A. Jarmola, and D. Budker, *Physical Review B* **87**, 014115 (2013).
- ⁴⁰A. Dréau, M. Lesik, L. Rondin, P. Spinicelli, O. Arcizet, J.-F. Roch, and V. Jacques, *Physical Review B* **84**, 195204 (2011).
- ⁴¹B. Yang, M. Dong, W. He, Y. Liu, C. Feng, Y. Wang, and G. Du, *IEEE Transactions on Microwave Theory and Techniques*, **1** (2019).
- ⁴²J. Wang, Y. Zhou, X. Zhang, F. Liu, Y. Li, K. Li, Z. Liu, G. Wang, and W. Gao, *Physical Review Applied* **7**, 064021 (2017).